Effects of interstitial carbon on the radiation tolerance of carbon-doped NiFe binary alloys from atomistic simulations

Guojia Ge[a], Feida Chen[a,b], Xiaobin Tang[a,b,*], Hai Huang[a], Jiwei Lin[a,c], Shangkun Shen[a], Jing Gao[a]

[a] Department of Nuclear Science & Technology, Nanjing University of Aeronautics and Astronautics, Nanjing 211106, China
[b] Key Laboratory of Nuclear Technology Application and Radiation Protection in Astronautics, Ministry of Industry and Information Technology, China
[c] Shanghai Nuclear Engineering Research & Design Institute, Shanghai 200233, China

ARTICLE INFO

ABSTRACT

Atomistic simulations were utilized to investigate the effects of interstitial carbon on the radiation tolerance of carbon-doped NiFe binary alloy (NiFeC). Cascade simulation and defect insertion method were implemented to systematically study the radiation-induced defect generation and clustering mechanisms. Results showed that the interstitial carbon reduced the defect counts during the thermal spike expansion in the ballistic stage. For the final survived defect clusters, the cluster size in NiFeC decreased significantly relative to that in NiFe alloy. The energetic and kinetic calculations verified the migration behavior of the interstitial and vacancy in NiFeC. The mobility of the interstitial was inhibited by the lattice distortion aggravated by interstitial carbon. The vacancy tended to bind with the carbon atoms and remained immobile. Both characteristics suppressed the formation of large-sized clusters, such as dislocation loop and stacking fault tetrahedra observed in NiFe.

1. Introduction

In contrast to conventional alloys, single-phase concentrated solid solution alloys (SP-CSAs), including high-entropy alloys, are composed of multiple principal elements but form simple crystal structure [1]. The unique design strategy of SP-CSAs provides possibilities to obtain exceptional properties, such as an excellent combination of strength and ductility, high thermodynamic stability, superior resistance to corrosion and radiation [2–5]. Different from the widely used strategy of introducing extrinsic defect sinks [6,7], SP-CSAs exhibit excellent radiation tolerance attributed to their high compositional complexity. The intrinsic lattice distortion and sluggish diffusion arising from compositional complexity can significantly modify defect kinetics and heat dissipation, suppressing radiation-induced damage accumulation [8–11]. Jin et al. compared the swelling properties between the single face-centered cubic (FCC) phase FeCoCrMnNi and pure Ni by using 5 MeV Ni ion irradiation at 500 ℃. The volume swelling of FeCoCrMnNi (0.2%) was 30 times lower than that of Ni (~6.7%) [8]. Lu et al. showed that the magnitude of segregation at radiation-induced dislocation loops was minimized in CoCrFeNiMn at 500 ℃ under 3 MeV Ni^{2+} irradiation conditions [9]. Lu et al. reported a new single-phase body-centered cubic structured Ti$_2$ZrHfV$_{0.5}$Mo$_{0.2}$, which exhibited scarce irradiation hardening after helium-ion irradiation [10]. These studies mainly focused on radiation-resistant enhancement through adding metallic elements but were limited to the substitutional solid solution strengthening.

Interstitial strengthening offers another route to achieve improvements both in the mechanical properties and radiation tolerance. Interstitial solute atoms, such as C, N, and B, even have more contributions to solid solution strengthening in comparison with substitutional solute atoms [12–14]. Recent studies successfully produced single FCC interstitial strengthening SP-CSAs with carbon dissolved up to 1.84 at.% [15]. Yield strength and ultimate tensile strength increased remarkably in the carbon-doped SP-CSAs because of the transformed fracture mechanism induced by interstitial carbon. Meanwhile, interstitial carbon may modify the atomic-level chemistry disorder and introduce lattice distortion larger than the substitution of solute atoms, thus strengthening the radiation tolerance of SP-CSAs. In the present work, the effects of interstitial carbon on the evolution of defects induced by irradiation were studied using an atomistic simulation method.

Although early studies on carbon-doped SP-CSAs mainly focused on alloys containing five elements. Evidences suggested that SP-CSAs' excellent properties, including sluggish diffusion, do not necessarily require a large number of alloying elements [16–18]. Considering the limit of atomistic potential, this study selected equiatomic NiFe as a matrix model. The effects of interstitial carbon on radiation-induced defect generation and evolution were investigated using displacement

cascade simulation and defect insertion method. These results illustrated the role of interstitial carbon on radiation tolerance of carbon-doped SP-CSAs.

2. Simulation methodology

Given that the octahedral site is the most stable site for the carbon interstitial. The carbon-doped NiFe binary alloy (NiFeC) was modeled by placing carbon atoms randomly at the octahedral sites of the FCC NiFe lattice (Fig. 1). In accordance with previous studies [19,20], different lattice constants were set to model NiFeC with varying concentrations of carbon. Specifically, 3.583, 3.586, 3.596, and 3.61 Å for NiFe with 0, 0.1 at.% C (NiFe0.1C), 0.5 at.% C (NiFe0.5C), and 1 at.% C (NiFe1C). The embedded atom method potential developed by Bonny et al. [21] was used to describe the interactions between Ni atoms and Fe atoms. Fe–C interactions were described using the Tersoff/ZBL potential developed by Henriksson et al. [22]. Considering that the Ni–C interaction is weaker than the Fe–C interaction, 12–6 Lennarde–Jones type of van der Waals interaction was adopted to describe the Ni–C interactions, which has been successfully used in irradiation damage studies of other metal–C systems [23,24]. All calculations were performed with the molecular dynamics (MD) code LAMMPS [25].

A system with the size of $30\ a_0 \times 30\ a_0 \times 30\ a_0$ (a_0 is the lattice constant) was used for cascade simulations. Initially, each model was relaxed at the NVT ensemble for 10 ps at 300 K until it reached a stable state. Subsequently, a primary knock-on atom (PKA) was given kinetic energy of 3 keV in the [1 3 5] direction and run at the NVE ensemble with a time step of 10^{-4} ps for 3 ps. Then additional 30 ps with a larger time step of 10^{-3} ps. Finally, the system was cooled down to 300 K until no energetic interactions remained in the system. In addition, 10 independent cascade simulations were performed in each model to reduce the statistical errors in the results. Cascade simulation can effectively present energetic ballistic events and the effects of thermal spike on defect production. However, the iterative time step should be small to accurately capture atomic forces during the ballistic stage. Because the kinetic energy of PKA is rapidly deposited and the atoms come close to one another. As a result, the cumulative irradiation damage simulated by overlapping single cascades is computationally expensive.

A defect insertion method was adopted to simulate the evolution of large-number defects that accumulated under irradiation [26,27]. This method bypasses the ballistic stage and accelerates microstructure evolution by creating overconcentration defects. In comparison with cascade simulation, the defect insertion approach significantly decreases the time needed to simulate the same degree of radiation damage. Several studies replicated 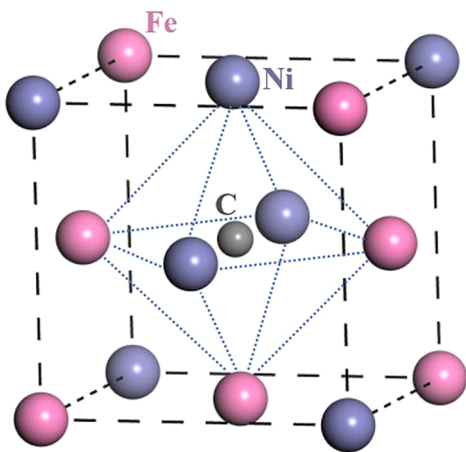the experimentally observed results by adopting this approach [28–31]. A small model ($20\ a_0 \times 20\ a_0 \times 20\ a_0$) was used to reveal the underlying clustering mechanisms. 1 at.% Frenkel pairs, vacancies, and interstitials were introduced into the model separately and relaxed in the isothermal isobaric ensemble at zero pressure.

The calculation results were visualized with OVITO. Wigner–Seitz (WS) cell method [32] was used to analyze the point defects. This approach is good for substitutional solid solutions and requires modification in the presence of impurity interstitial atoms. In the present study, WS analysis was performed only for nickel and iron atoms, carbon atoms were not considered so that interstitial carbon could not be interpreted as a point defect. The cluster size distribution was analyzed by calculating the distance between each defect and all other defects. Defects within a fixed cutoff distance (3.6 Å) from each other were interpreted as a part of the same defect cluster. Both the WS analysis and Cluster analysis used here have been implemented in OVITO. In addition, the kinetic (mean square displacements, MSD) and energetic (formation energy, E_f) properties of point defects were calculated to reveal the role of interstitial carbon. MSD and E_f can be respectively obtained as follows:

$$\mathrm{MSD} = \frac{1}{N} \sum_{i=1}^{N} \left[\vec{r_i}(t) - \vec{r_i}(0) \right]^2 \tag{1}$$

$$E_f^\alpha = E_{tot}^\alpha - E_{tot} \pm E_{coh} \tag{2}$$

where $\vec{r_i}(t)$ refers to the atom position of the point defect at time t and i is the ith time interval for the trajectory in Eq. (1). The positive (or negative) sign in Eq. (2) corresponds to the vacancy (or interstitial) at a particular site α. E_{tot}^α (E_{tot}) is the total energy of the system with (or without) the point defect. E_{coh} is the cohesive energy (per atom) in the system [33].

3. Results and discussion

3.1. Displacement cascades

Fig. 2 shows the time evolution of the number of point defects in NiFe doped with different carbon concentrations during displacement cascades. The defects rapidly reached a peak due to the transient localized melting caused by energetic PKA in the form of a thermal spike. Followed by cooling and partial recrystallization, they considerably decreased compared with the peak value. The difference in the final stable defect number between NiFe and NiFeC was negligible (see the
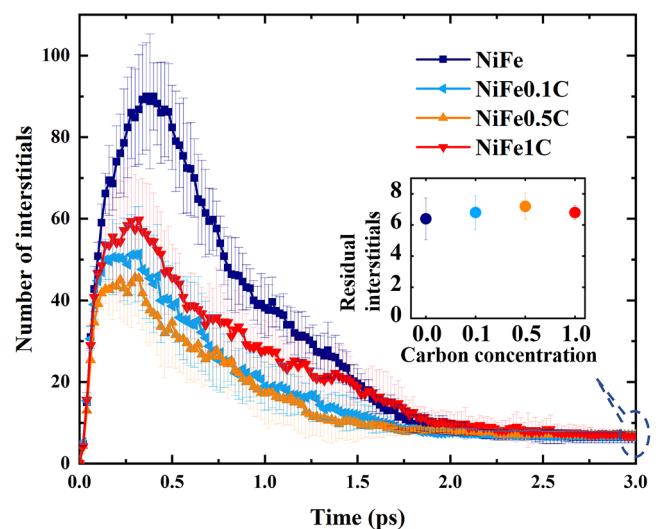

Fig. 1. Atomic structure of NiFeC. The carbon atom (gray) lies in the octahedral site, and Ni atoms (purple) and Fe atoms (pink) are randomly placed to replicate the random nature of SP-CSAs.

Fig. 2. Time evolution of the number of interstitials in NiFe, NiFe0.1C, NiFe0.5C, and NiFe1C during the displacement cascades. The number of final stable interstitials is shown in the inset.

inset in Fig. 2), suggesting that adding interstitial carbon exerts no noticeable effect. This result agrees with the null effect of carbon at its concentration on the number of survived defects in previous cascades simulations [34,35]. Whereas, the advanced thermal spike and reduced defect peak value during ballistic stage were found in the systems added with interstitial carbon.

Previous studies revealed that the thermal spike is inhibited or absented in graphite during the cascades simulation owing to the high displacement energy and atomization enthalpy of graphite [36,37]. In the present work, the advanced thermal spike and the reduction of defects in NiFeC may be attributed to the role of carbon atoms in inhibiting the expansion of thermal spike. During the ballistic stage, the systems added with interstitial carbon have greater atomic density and lattice distortion, thereby shortening the mean free path of displaced atoms. The energy deposited more rapidly in the matrix, thus making the thermal spike time advanced. In the meanwhile, owing to the interstitial carbon atoms also absorb a portion of the energy of PKA, the energy delivered to metal atoms is reduced. Hence, the defects generated in the ballistic stage were decreased by the addition of interstitial carbon. According to this, the reduced defects number is supposed to be positively correlated with carbon concentration. However, NiFe0.5C presented the best radiation response in this work with the lowest defect generation during the ballistic stage. This phenomenon is supposed to be the result of two competitive factors: on the one hand, carbon atoms absorbing the energy of PKA and reducing the defect generation of Fe and Ni atoms. On the other hand, the displaced carbon continues to produce lattice distortion, making the adjacent atoms deviated from their original lattice sites. Such distortion is counted as defects by WS method.

As shown in Fig. 2, the number of point defects produced by NiFe was greater than that produced by NiFeC in the course of the ballistic stage. However, the number of defects after the kinetic stage almost did not differ. This finding indicates that the kinetic stage plays a dominant role in the evolution of defects. The kinetic stage was investigated in the subsequent study via the defect insertion method. The influence of the displaced carbon on the number of defects could be eliminated. As such, the effect of interstitial carbon on defect migration and recombination behavior could be accurately reflected.

3.2. Frenkel pair evolution

The systems containing 1 at.% randomly distributed Frenkel pairs (320 interstitials and 320 vacancies) were run for 5 ns at 300 K. Given that the vacancies hardly moved at this temperature and the number of residual vacancies was equal to that of the interstitials. Therefore, only the interstitial clusters were calculated. The number of interstitials in different cluster size distributions and the total amount of NiFe alloys with different carbon concentrations are shown in Fig. 3. A positive correlation between annihilated defect number and carbon concentration was evident. The higher the carbon concentration in the system was, the fewer the residual defects were. This finding suggests that interstitial carbon may play a role of enhancing the recombination of Frenkel pairs.

The difference in cluster size distributions between NiFe and NiFeC was significant. Interstitials prefer to form clusters, and several clusters containing more than 10 interstitial atoms formed in NiFe, leaving a small number of single interstitials. The number of larger-sized clusters apparently decreased in NiFeC, even there is no cluster containing more than 10 interstitials formed in NiFe1C. This finding indicates another role of interstitial carbon under irradiation, which is effectively inhibiting the formation of large defect clusters. Through such function, the interstitial carbon also modifies the recombination of point defects. The mobility of interstitials is restrained after they form clusters, thereby excluding them from recombining with vacancies [38]. Thus, the obstruction for interstitials to form a cluster induced by carbon increases their probability to recombine with vacancies nearby. These

results clarify the effect of interstitial carbon on defect recombination and cluster formation. The essential determinants of these behaviors are the mobility and diffusion pathway of interstitials and vacancies, which will be further studied in subsequent sections.

3.3. Interstitial diffusion at different temperatures

An important feature of the defect insertion method is that the types of defects are controllable. Such as interstitial kinetics, including their migrating behaviors and clustering processes, could be explored by introducing interstitial type defects only. The 1 at.% interstitials were randomly distributed in the models, and the simulations were run for 5 ns at 300 K, 500 K, and 700 K. The numbers of interstitials in different cluster size distributions of NiFe and NiFe0.5C are shown in Fig. 4. The cluster size distribution of interstitials was relatively uniform at 300 K in NiFe. As the temperature increases, the interstitials apparently translated from the clusters containing few atoms to more than 50 atoms. At 700 K, almost all interstitials formed a large-sized cluster due to the accelerated diffusion of interstitials at high temperatures. The same transition trend occurred in NiFeC, but the overall size distribution of the clusters was considerably smaller than that of NiFe. At 700 K, only a small number of interstitials formed clusters of more than 50 atoms. The interstitial kinetics toward cluster formation in NiFeC alloy appear to be slower than that in NiFe, suggesting that the mobility of interstitials is definitely inhibited by interstitial carbon.

The distribution of interstitial cluster size in NiFe or NiFeC changed obviously after the temperature increased from 300 K to 500 K. The interstitials in the two systems were visualized after relaxation at 500 K. A large interstitial cluster was found at the center of NiFe, as shown in Fig. 5(a), and it was an interstitial dislocation loop identified via dislocation analysis (DXA) [39]. Interstitial clusters in NiFeC were considerably smaller than that in NiFe. They hardly move to interact with each other, thus there is no further formation of larger clusters. In previous studies, simulations and experiments demonstrated that the addition of other metal elements (Fe, Cr, and Mn) in pure Ni to form SP-CSAs increases migration barriers and decreases overall diffusivity, leading to a slow defect cluster formation during irradiation [17,20]. The results presented here appear that adding interstitial carbon had a similar effect. MSD calculations were performed to quantify the mobility of the interstitials, and the results showed the value of MSD in NiFe is about three times of that in NiFeC (9.08 and 2.95 Å for NiFe and NiFeC in 5 ns respectively). Therefore, interstitial carbon is able to further enhance the sluggish diffusion effect by turning the composition complexity of SP-CSAs. Then suppressing the formation of large interstitial clusters, such as dislocation loops.

3.4. Vacancy diffusion

The vacancies were completely immobile on the MD timescales until 700 K, started to diffuse at 1000 K, and fully diffused at 1200 K in pure Ni [26]. Therefore, 1200 K was set as the simulation temperature to capture vacancy evolution. Fig. 6 shows the distribution of vacancies in NiFe and NiFeC at 20 ns. In contrast to most vacancies that migrated and aggregated to form clusters in NiFe, there is a significant number of individual vacancies in NiFeC. It is worth noting that stacking fault tetrahedra (four triangular planes bounded by six stair-rod partial dislocations) was found in NiFe, which can be formed merely through the aggregation of vacancies as confirmed in Aidhy's study [26]. Similar to the interstitial evolution, the vacancy kinetics toward cluster formation in NiFeC was slower than that in NiFe. In Lu's study [5], the migration energy barrier of a single vacancy in NiFe was slightly lower than that in pure Ni and associated with the size difference of the atoms in the alloy. As such, the lattice distortion effect would accelerate vacancy migration, which contrasted with the phenomena observed in the present study.

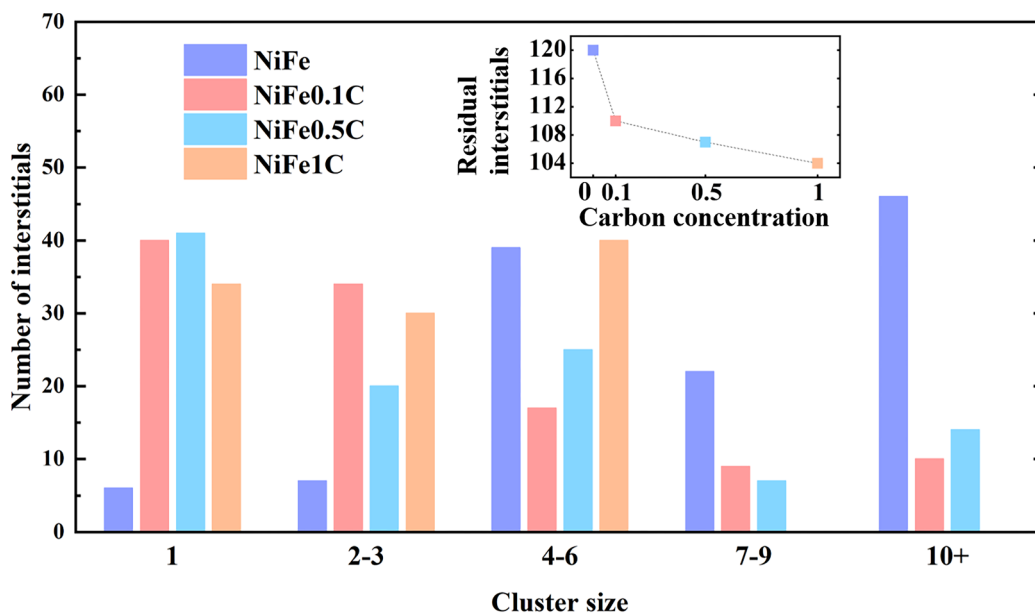The formation energy E_f^v at varying distances away from the

Fig. 3. Number of interstitials in different cluster size distributions of NiFe, NiFe0.1C, NiFe0.5C, and NiFe1C after 5 ns relaxation. The number of total interstitials is shown in the inset.
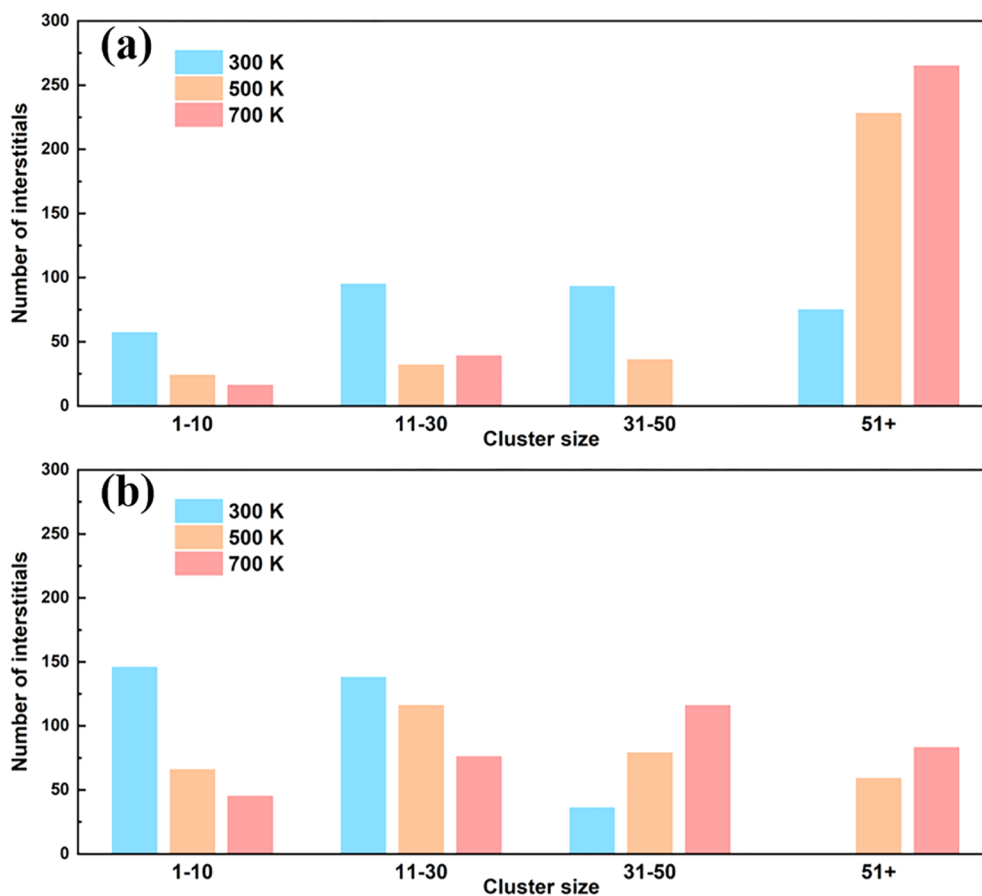

Fig. 4. Numbers of interstitials in different cluster-size distributions of (a) NiFe and (b) NiFe0.5C at 300 K, 500 K, and 700 K after 5 ns relaxation.

interstitial carbon was calculated to understand the interaction between interstitial carbon and vacancy. When vacancy formed in the matrix, $E_f^v = 1.51$ eV. When vacancy formed adjacent to the interstitial carbon, $E_f^v = 1.35$ eV. E_f^v adjacent to interstitial carbon was lower than that in the matrix, indicating that the vacancy can be easily trapped by carbon

atoms. The interstitial carbon occupying the octahedral site in the equilibrium lattice is scarcely moved. Thus, when the vacancy and carbon atom combined and formed a vacancy–carbon complex, their mobility was significantly inhibited. Rigorous ab initio calculations confirmed that interstitial carbon is strongly bound to a single vacancy
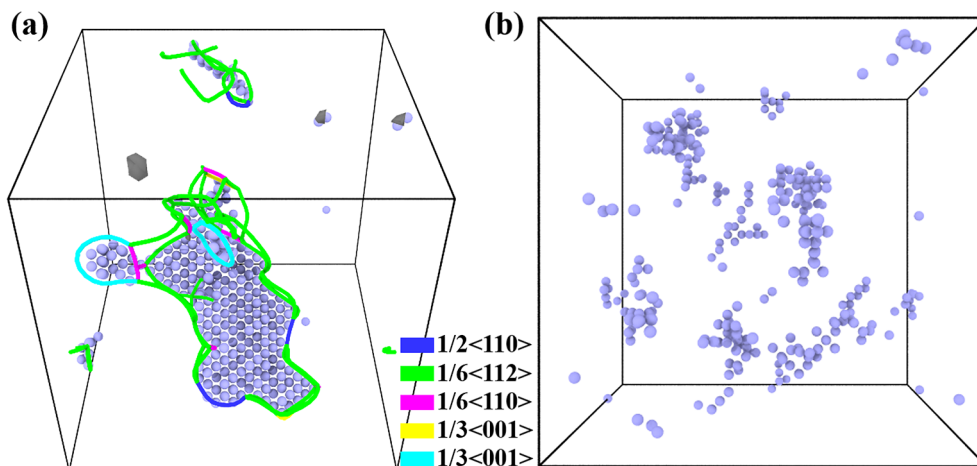
Fig. 5. Interstitials (blue balls) distribution of (a) NiFe and (b) NiFe0.5C after 5 ns relaxation. The colored lines represent dislocations identified via DXA, and the grey meshes represent defect meshes.

[40,41]. In the present study, the mobility of the vacancies and small vacancy clusters was restrained by the amount of interstitial carbon dissolved in the matrix, resulting in no SFT formation.

4. Conclusions

NiFeC models with different concentrations of carbon atoms occupying octahedral sites were built for MD simulation. The role of interstitial carbon in SP-CSAs under irradiation was explored, and the radiation tolerance of carbon-doped SP-CSAs was evaluated. The cascade simulation captured energetic ballistic events, including shock waves and thermal spikes. The defect insertion method simulates the evolution of large-number defects with low computation cost. Both methods were applied to systematically study the radiation-induced defect generation and clustering mechanisms. The conclusions drawn are as follows:

1) A significant reduction of the defects number in the thermal spike

was found in NiFeC. It is attributed to the role of interstitial carbon in inhibiting the expansion of the thermal spike.

2) With the increasing of interstitial carbon concentration, the survived point defects in the systems inserted 1 at.% Frenkel pairs became fewer. And the size of the interstitial cluster also became smaller. The formation of clusters restrained the migration of the defects and reduced the probability of recombination.

3) MSD calculation demonstrated that the mobility of interstitial was inhibited in NiFeC. Vacancy tended to bind with the carbon atoms and became immobile. The reduced mobility of point defects suppressed the formation of large-sized clusters, such as dislocation loop and stacking fault tetrahedra observed in NiFe.

The effects of interstitial carbon found in NiFeC alloys may provide a promising method for carbon-doped SP-CSAs to obtain promoted irradiation tolerance and prevent material degradation in extreme radiation environments.
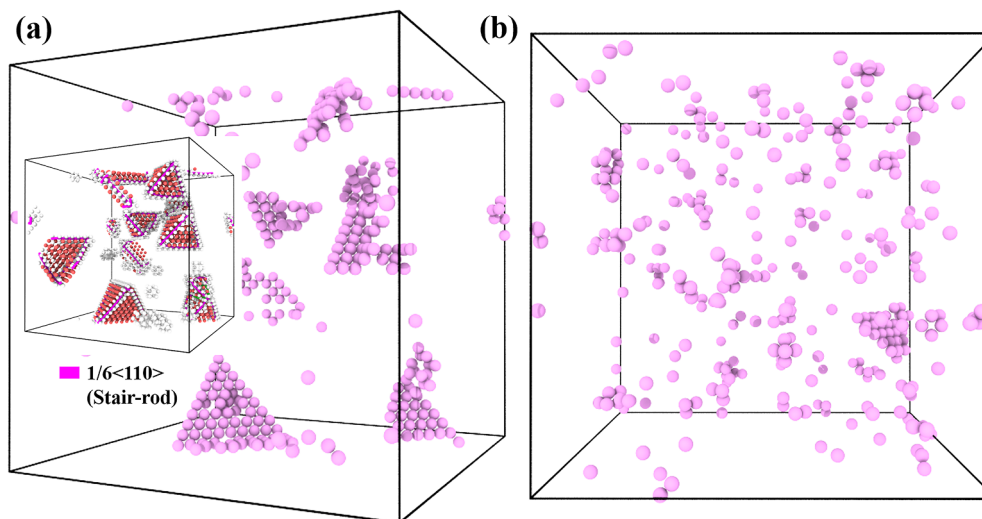

Fig. 6. Vacancies (light-red balls) distribution of (a) NiFe and (b) NiFe0.5C after 20 ns relaxation, the inset is the stacking fault tetrahedra identified via DXA (red line represents stair-rod dislocation line) and common neighbor analysis (red ball represents hcp structure).

CRediT authorship contribution statement

Guojia Ge: Conceptualization, Methodology, Software, Validation, Formal analysis, Investigation, Data curation, Writing - original draft, Writing - review & editing. **Feida Chen:** Conceptualization, Writing - original draft, Funding acquisition. **Xiaobin Tang:** Writing - original draft, Supervision, Project administration, Funding acquisition. **Hai Huang:** Methodology, Writing - original draft. **Jiwei Lin:** Investigation. **Shangkun Shen:** Investigation. **Jing Gao:** Investigation.

Declaration of Competing Interest

The authors declare that they have no known competing financial interests or personal relationships that could have appeared to influence the work reported in this paper.

Acknowledgement

References

[1] J.W. Yeh, S.K. Chen, S.J. Lin, J.Y. Gan, T.S. Chin, T.T. Shun, C.H. Tsau, S.Y. Chang, Nanostructured high-entropy alloys with multiple principal elements: novel alloy design concepts and outcomes, Adv. Eng. Mater. 6 (5) (2004) 299–303.

[2] Y. Chou, J. Yeh, H. Shih, The effect of molybdenum on the corrosion behaviour of the high-entropy alloys $Co_{1.5}CrFeNi_{1.5}Ti_{0.5}Mo_x$ in aqueous environments, Corros. Sci. 52 (8) (2010) 2571–2581.

[3] B. Gludovatz, A. Hohenwarter, D. Catoor, E.H. Chang, E.P. George, R.O. Ritchie, A fracture-resistant high-entropy alloy for cryogenic applications, Science 345 (6201) (2014) 1153–1158.

[4] J. He, H. Wang, H. Huang, X. Xu, M. Chen, Y. Wu, X. Liu, T. Nieh, K. An, Z. Lu, A precipitation-hardened high-entropy alloy with outstanding tensile properties, Acta Mater. 102 (2016) 187–196.

[5] C. Lu, L. Niu, N. Chen, K. Jin, T. Yang, P. Xiu, Y. Zhang, F. Gao, H. Bei, S. Shi, Enhancing radiation tolerance by controlling defect mobility and migration pathways in multicomponent single-phase alloys, Nat. Commun. 7 (2016) 13564.

[6] F. Chen, X. Tang, Y. Yang, H. Huang, J. Liu, H. Li, D. Chen, Atomic simulations of Fe/Ni multilayer nanocomposites on the radiation damage resistance, J. Nucl. Mater. 468 (2016) 164–170.

[7] X. Sun, F. Chen, H. Huang, J. Lin, X. Tang, Effects of interfaces on the helium bubble formation and radiation hardening of an austenitic stainless steel achieved by additive manufacturing, Appl. Surf. Sci. 467–468 (2019) 1134–1139.

[8] K. Jin, C. Lu, L. Wang, J. Qu, W. Weber, Y. Zhang, H. Bei, Effects of compositional complexity on the ion-irradiation induced swelling and hardening in Ni-containing equiatomic alloys, Scr. Mater. 119 (2016) 65–70.

[9] C. Lu, T. Yang, K. Jin, N. Gao, P. Xiu, Y. Zhang, F. Gao, H. Bei, W.J. Weber, K. Sun, Radiation-induced segregation on defect clusters in single-phase concentrated solid-solution alloys, Acta Mater. 127 (2017) 98–107.

[10] Y. Lu, H. Huang, X. Gao, C. Ren, J. Gao, H. Zhang, S. Zheng, Q. Jin, Y. Zhao, C. Lu, A promising new class of irradiation tolerant materials: $Ti_2ZrHfV_{0.5}Mo_{0.2}$ high-entropy alloy, J. Mater. Sci. Technol. 35 (3) (2019) 369–373.

[11] T. Yang, C. Li, S.J. Zinkle, S. Zhao, H. Bei, Y. Zhang, Irradiation responses and defect behavior of single-phase concentrated solid solution alloys, J. Mater. Res. 33 (19) (2018) 3077–3091.

[12] N. Stepanov, D. Shaysultanov, R. Chernichenko, N.Y. Yurchenko, S. Zherebtsov, M. Tikhonovsky, G. Salishchev, Effect of thermomechanical processing on microstructure and mechanical properties of the carbon-containing CoCrFeNiMn high entropy alloy, J. Alloy. Compd. 693 (2017) 394–405.

[13] Z. Wang, I. Baker, W. Guo, J.D. Poplawsky, The effect of carbon on the microstructures, mechanical properties, and deformation mechanisms of thermo-mechanically treated $Fe_{40.4}Ni_{11.3}Mn_{34.8}Al_{7.5}Cr_6$ high entropy alloys, Acta Mater. 126 (2017) 346–360.

[14] Z. Wu, C. Parish, H. Bei, Nano-twin mediated plasticity in carbon-containing FeNiCoCrMn high entropy alloys, J. Alloy. Compd. 647 (2015) 815–822.

[15] J.Y. Ko, S.I. Hong, Microstructural evolution and mechanical performance of carbon-containing CoCrFeMnNi-C high entropy alloys, J. Alloy. Compd. 743 (2018) 115–125.

[16] B. Gludovatz, A. Hohenwarter, K.V. Thurston, H. Bei, Z. Wu, E.P. George, R.O. Ritchie, Exceptional damage-tolerance of a medium-entropy alloy CrCoNi at cryogenic temperatures, Nat. Commun. 7 (2016) 10602.

[17] K. Jin, C. Zhang, F. Zhang, H. Bei, Influence of compositional complexity on interdiffusion in Ni-containing concentrated solid-solution alloys, Materials Research Letters 6 (5) (2018) 293–299.

[18] C. Zhang, F. Zhang, K. Jin, H. Bei, S. Chen, W. Cao, J. Zhu, D. Lv, Understanding of the elemental diffusion behavior in concentrated solid solution alloys, Journal of Phase Equilibria and Diffusion 38 (4) (2017) 434–444.

[19] Z. Wang, I. Baker, Z. Cai, S. Chen, J.D. Poplawsky, W. Guo, The effect of interstitial carbon on the mechanical properties and dislocation substructure evolution in $Fe_{40.4}Ni_{11.3}Mn_{34.8}Al_{7.5}Cr_6$ high entropy alloys, Acta Mater. 120 (2016) 228–239.

[20] Y. Zhang, G.M. Stocks, K. Jin, C. Lu, H. Bei, B.C. Sales, L. Wang, L.K. Béland, R.E. Stoller, G.D. Samolyuk, Influence of chemical disorder on energy dissipation and defect evolution in concentrated solid solution alloys, Nat. Commun. 6 (2015) 8736.

[21] G. Bonny, N. Castin, D. Terentyev, Interatomic potential for studying ageing under irradiation in stainless steels: the FeNiCr model alloy, Modell. Simul. Mater. Sci. Eng. 21 (8) (2013) 085004.

[22] K. Henriksson, C. Björkas, K. Nordlund, Atomistic simulations of stainless steels: a many-body potential for the Fe–Cr–C system, J. Phys.: Condens. Matter 25 (44) (2013) 445401.

[23] H. Huang, X. Tang, F. Chen, F. Gao, Q. Peng, L. Ji, X. Sun, Self-healing mechanism of irradiation defects in nickel–graphene nanocomposite: An energetic and kinetic perspective, J. Alloy. Compd. 765 (2018) 253–263.

[24] Y. Kim, J. Baek, S. Kim, S. Kim, S. Ryu, S. Jeon, S.M. Han, Radiation resistant vanadium-graphene nanolayered composite, Sci. Rep. 6 (2016) 24785.

[25] S. Plimpton, Fast parallel algorithms for short-range molecular dynamics, J. Comput. Phys. 117 (1) (1995) 1–19.

[26] D.S. Aidhy, C. Lu, K. Jin, H. Bei, Y. Zhang, L. Wang, W.J. Weber, Point defect evolution in Ni, NiFe and NiCr alloys from atomistic simulations and irradiation experiments, Acta Mater. 99 (2015) 69–76.

[27] P.M. Derlet, S.L. Dudarev, Microscopic structure of a heavily irradiated material, Physical Review Materials 4 (2) (2020).

[28] D.S. Aidhy, Y. Zhang, W.J. Weber, Radiation damage in cubic ZrO_2 and yttria-stabilized zirconia from molecular dynamics simulations, Scr. Mater. 98 (2015) 16–19.

[29] A.H. Quadery, S. Pacheco, A. Au, N. Rizzacasa, J. Nichols, T. Le, C. Glasscock, P.K. Schelling, Atomic-scale simulation of space weathering in olivine and orthopyroxene, J. Geophys. Res. Planets 120 (4) (2015) 643–661.

[30] Y. Zhang, D.S. Aidhy, T. Varga, S. Moll, P.D. Edmondson, F. Namavar, K. Jin, C.N. Ostrouchov, W.J. Weber, The effect of electronic energy loss on irradiation-induced grain growth in nanocrystalline oxides, PCCP 16 (17) (2014) 8051–8059.

[31] A. Chartier, M.C. Marinica, Rearrangement of interstitial defects in alpha-Fe under extreme condition, Acta Mater. 180 (2019) 141–148.

[32] K. Nordlund, M. Ghaly, R.S. Averback, M. Caturla, T.D. De La Rubia, J. Tarus, Defect production in collision cascades in elemental semiconductors and fcc metals, Physical Review B 57 (13) (1998) 7556.

[33] X. Li, W. Liu, Y. Xu, C. Liu, Q. Fang, B. Pan, J.-L. Chen, G.-N. Luo, Z. Wang, An energetic and kinetic perspective of the grain-boundary role in healing radiation damage in tungsten, Nucl. Fusion 53 (12) (2013) 123014.

[34] A.F. Calder, D.J. Bacon, A.V. Barashev, Y.N. Osetsky, Computer simulation of cascade damage in α-iron with carbon in solution, J. Nucl. Mater. 382 (2–3) (2008) 91–95.

[35] M.Y. Tikhonchev, V. Svetukhin, A. Kadochkin, E. Gaganidze, Molecular dynamics simulation of atomic displacement cascades in Fe-9 at% Cr and Fe-9 at% Cr-0.1 at% C alloys, Russian Metallurgy (Metally) 2011 (5) (2011) 415.

[36] H. Christie, M. Robinson, D. Roach, D. Ross, I. Suarez-Martinez, N. Marks, Simulating radiation damage cascades in graphite, Carbon 81 (2015) 105–114.

[37] H. Huang, X. Tang, F. Chen, J. Liu, D. Chen, Role of graphene layers on the radiation resistance of copper–graphene nanocomposite: Inhibiting the expansion of thermal spike, J. Nucl. Mater. 493 (2017) 322–329.

[38] H.-S. Do, B.-J. Lee, Origin of radiation resistance in multi-principal element alloys, Sci. Rep. 8 (1) (2018) 16015.

[39] A. Stukowski, V.V. Bulatov, A. Arsenlis, Automated identification and indexing of dislocations in crystal interfaces, Modell. Simul. Mater. Sci. Eng. 20 (8) (2012) 085007.

[40] C. Barouh, T. Schuler, C.-C. Fu, M. Nastar, Interaction between vacancies and interstitial solutes (C, N, and O) in α − Fe: from electronic structure to thermodynamics, Physical Review B 90 (5) (2014) 054112.

[41] C. Domain, C. Becquart, J. Foct, Ab initio study of foreign interstitial atom (C, N) interactions with intrinsic point defects in α-Fe, Physical Review B 69 (14) (2004) 144112.